Rapid Reduction of Hg(II) by Mercuric Ion Reductase Does Not Require the Conserved C-Terminal Cysteine Pair Using $HgBr_2$ as the Substrate†

Stefan Engst* and Susan M. Miller*

Department of Pharmaceutical Chemistry, University of California, San Francisco, California 94143-0446

Received April 10, 1998; Revised Manuscript Received June 3, 1998

ABSTRACT: Conditions are described under which the nonphysiological substrate mercuric bromide ($HgBr_2$) is rapidly turned over, both by the wild type (CCCC) and by an active site double mutant (CCAA) of mercuric reductase in which the C-terminal cysteines 557′ and 558′ are replaced by alanine and only the redox-active pair Cys135 and Cys140 are available for catalysis. A maximum rate of turnover k_{cat}^{app} of ≈18 s^{-1} (at 3 °C) for both enzymes is observed, and at high [$HgBr_2$]/[enzyme] ratios, inhibition is found. The UV−vis spectral changes during turnover are closely similar in both enzymes, indicating that catalysis follows the same enzymatic mechanism. Single-turnover analysis of the mutant enzyme shows that after binding of $HgBr_2$, two further rapid events ensue, followed by reduction of the metal ion (k_{obs} ≈ 23.5 s^{-1}). It is shown that under multiple-turnover conditions, completion of the catalytic cycle must occur via an ordered mechanism where rapid binding of a new molecule of $HgBr_2$ to EH_2·$NADP^+$ precedes exchange of the pyridine nucleotide. Binding of $HgBr_2$ to the active site triple mutant C135A/C557A/C558A (ACAA) is ca. 100-fold slower compared to that of the CCAA mutant and results in no detectable turnover. It is concluded that in the reducible enzyme·Hg(II) complex, the metal ion is coordinated to Cys135 and Cys140 and that for efficient catalysis both residues are required. Furthermore, the data imply that binding to EH_2·NADPH occurs via initial rate-limiting attack of Cys135, followed by reaction with Cys140.

Mercuric reductase (MR),[1] one of the key components in the predominant bacterial detoxification pathway of mercurials, catalyzes the two-electron reduction of Hg(II) shown in eq 1.

$$Hg(SR)_2 + NADPH + H^+ \rightarrow Hg^0 + NADP^+ + 2RSH \quad (1)$$

The enzyme is a pyridine nucleotide:disulfide oxidoreductase and shares many structural and spectroscopic similarities with other group members such as glutathione reductase and lipoamide dehydrogenase. As part of their active sites, all members contain an FAD cofactor and a redox-active disulfide (cysteines 135 and 140 in MR from *Pseudomonas aeruginosa*, TN501). MR is unique in that in addition to this fully conserved cysteine pair, a second cysteine pair (cysteines 557 and 558), conserved only in mercuric ion reductases, is present in the active site (*1*). As shown in Scheme 1, MR can assume four distinct redox states, which are readily discernible with spectroscopic techniques (*2*, *3*). Not all of them are catalytically relevant; during regular turnover, the enzyme cycles only between the EH_2 form, in which all four cysteines are reduced and the flavin is oxidized, and the EH_4 form, which carries two additional redox equivalents that reside on either the flavin or the reduced pyridine nucleotide (*4*). A view of the reaction center derived from crystallographic data (*5*) for the enzyme from *Bacillus* sp. RC607 is shown in Scheme 2. The four cysteine residues in this enzyme (207, 212, 628′, and 629′) are located on the si side of the flavin and reflect the main components of the Hg(II) binding site. Of these cysteines, residue 212 (analogous to 140 in TN501) lies immediately below the flavin ring [2.97 Å, sulfur−flavin C(4a)] and Cys207 is found another 3.72 Å further below (sulfur−sulfur distance). The remaining two cysteines (628′ and 629′), which belong to the other subunit, are significantly further away from the flavin center; their sulfur−flavin C(4a) distances are 10.25 and 14.05 Å, respectively. In addition to the cysteines, two tyrosines, 264 and 605′, are also part of the metal substrate binding site (*5*). The overall topology of the binding pocket suggests at least two potential binding modes for Hg(II) close to the flavin ring that may occur during catalysis. In the first, the metal ion could be bound in a bicoordinate fashion between Cys212 and Cys207, thereby quenching the charge transfer interaction between flavin and Cys212 (Cys140 in TN501; see Scheme 1). In a second binding mode, tight ligation of Hg(II) between Cys207 and Cys628′ (sulfur−sulfur distance of 4.33 Å) and weaker interactions with the oxygens (O−O distance of 5.75 Å) of Tyr264 and Tyr605′ are envisioned. In crystallographic studies, Cd(II), a competitive inhibitor of MR, was found in the latter binding site (*5*).

† This work was supported by grants from NIGMS (GM50670), The Petroleum Research Foundation of the American Chemical Society (ACS-PRF 27532G4), and the UCSF Academic Senate.

* Inquiries to S.M.M.: telephone, (415) 476-7155; fax, (415) 476-0688; e-mail, smiller@cgl.ucsf.edu. Inquiries to S.E.: e-mail, engst@cgl.ucsf.edu.

[1] Abbreviations: CT, charge transfer; EH_2, two-electron reduced enzyme where the redox-active cysteines are reduced and the flavin is oxidized; EH_2·NADPH, two-electron reduced enzyme complexed with NADPH; ME, 2-mercaptoethanol; MR, mercuric ion reductase; $NADP^+$, nicotinamide adenine dinucleotide phosphate; NADPH, reduced nicotinamide adenine dinucleotide phosphate; RSH, thiol-containing compound such as ME or cysteine; SVD, singular value decomposition.

S0006-2960(98)00816-2 CCC: $15.00
Published on Web 07/29/1998

Scheme 1: Schematic View of the Redox States of Mercuric Reductase[a]

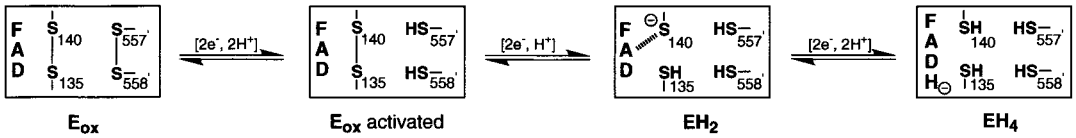

[a] The numbers refer to the active site cysteines in the sequence of MR from TN501. The corresponding residues in the sequence of the enzyme from *Bacillus* sp. RC607 are 207, 212, 628′, and 629′. The interrupted line between FAD and Cys140 in the EH_2 species symbolizes a charge transfer interaction.

Scheme 2: Schematic View of the Active Site of Mercuric Reductase (MR) from *Bacillus* sp. RC607 As Derived from Crystallographic Data[a]

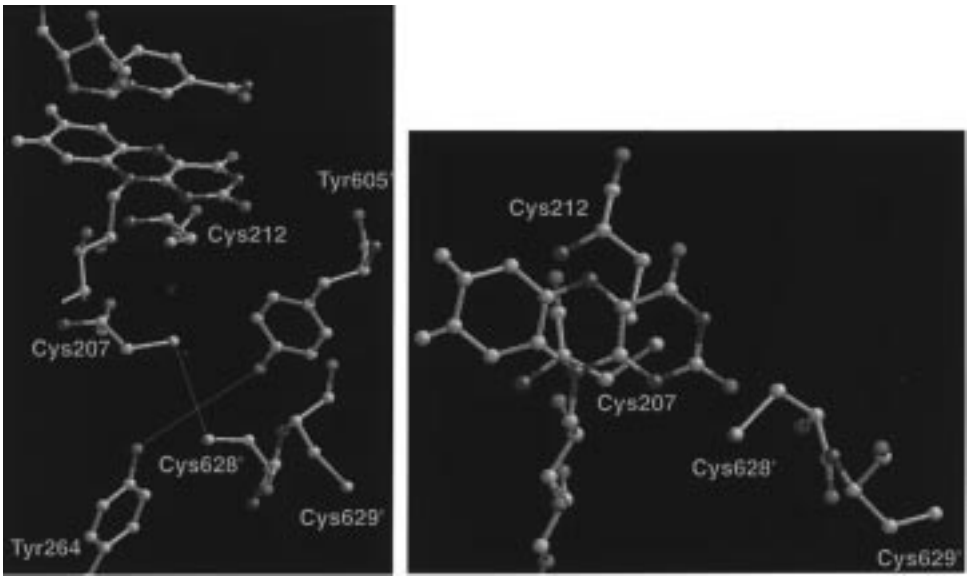

[a] (Left) Below the flavin ring, the four cysteine and two tyrosine residues which are part of the binding site of Hg(II) are shown. The green cross between Cys207 and Cys212 denotes a possible binding site for the metal ion. The intersection of the green lines connecting Cys207 and Cys628′, and Tyr264 and Tyr605′, is the approximate position in which a Cd(II) ion was found, after soaking crystals with this metal ion. Above the flavin ring, the nicotinamide portion of the pyridine nucleotide is shown. (Right) View of the four active site cysteines as seen from the nicotinamide binding site through the plane of the flavin ring system. Note that the Tyr residues are omitted for clarity.

To understand the role of the four active site cysteines, a series of single, double, and triple Cys to Ala mutants have previously been generated (*4*, *6*−*8*). Removal of either or both of the redox-active thiols (cysteine 135 or 140) essentially abolishes the enzyme's capacity to reduce Hg(II) in vivo as well as in standard in vitro catalytic assays using $Hg(SR)_2$ as the substrate (≤0.03% of the wild-type activity; *6*). These results strongly suggest that both cysteines of the redox-active pair play an essential role in the catalytic mechanism of Hg(II) reduction.

In contrast, removal of one or both C-terminal cysteines (557 and 558) results in variable behavior under the different conditions. In vivo studies have shown that mutation of either or both of the C-terminal residues to alanine leads to disruption of the Hg(II) detoxification pathway, and the cells become supersensitive to Hg(II) (*7*, *8*). Although all three mutants are lethal in vivo, in vitro studies demonstrated that catalysis is not equally abolished in all three. Like the redox-active Cys to Ala mutants, the double mutant C557A/C558A (CCAA)[2] is essentially inactive using $Hg(SR)_2$ as the substrate in typical in vitro assays (≤0.1% of the wild type activity; *7*). However, the single mutants C557A (CCAC) and C558A (CCCA) are less impaired, with k_{cat} values of 5 and 65−100% of the wild type activity, respectively, but an overall decrease in catalytic efficiency (k_{cat}/K_M) of 200- and 7-fold, respectively, compared to that of the wild type (*8*). While these data clearly demonstrate the requirement of the C-terminal cysteine pair for efficient reduction of $Hg(SR)_2$, it remains unclear whether the individual roles for these cysteines include participation in a catalytically reducible complex of Hg(II) or simply in the process of exchanging free thiol ligands for enzyme ligands. We have addressed this question by examining the ability of wild type and CCAA mutant enzymes to reduce alternative mercuric ion compounds. In this report, we describe conditions that unequivocally demonstrate that the CCAA double mutant is capable of rapidly reducing Hg(II) when $HgBr_2$ is used as the substrate.

[2] A four-letter code for wild type and active site mutants, which carry one or more mutations in position 135, 140, 557, and 558 (TN501 numbering) of the amino acid sequence, is used. For example, CCCC denotes the wild type enzyme with cysteines in all four positions. CCAA refers to a double mutant in which cysteines 557 and 558 are both replaced by alanine. (Note, Cys557 and Cys558 in the TN501 enzyme were previously referred to as 558 and 559, which is correct if the starting methionine is included. However, 135, 140, 557, and 558 are the consistent set of numbers for the mature protein.)

MATERIALS AND METHODS

Materials. Chymotrypsin (TLCK-treated, type VII) and glutathione reductase (from baker's yeast, type IV) were obtained from Sigma. All other chemicals were of the

highest grade available and were used without further purification.

Methods. For routine UV−visible absorbance measurements, spectra were recorded with a Shimadzu UV-2101PC double-beam spectrophotometer or a Hewlett-Packard 8452A diode array spectrophotometer. Rapid reaction studies were carried out at 3−4 °C using a stopped-flow sample handling unit (SF.17MV, 1 cm optical path) equipped with a 150 W xenon lamp, an optical filter with a cutoff limit at 315 nm, and a UV−visible diode array detector (all from Applied Photophysics). In its fastest mode, the diode array records spectra between 190 and 730 nm at intervals of 2.54 ms. This data aquisition mode was typically used for measurements in the visible region between 400 and 730 nm. Due to low lamp intensity in the near-UV region, the integration time was increased to 3−6 ms when changes at 340 nm were followed and the starting absorbance was >0.5. Data were analyzed either manually or using ProK (Applied Photophysics), a program that allows singular value decomposition (SVD) of the raw data and fitting to appropriate kinetic models. From this procedure, kinetic constants and spectral species were obtained. For the single-wavelength studies, the diode array detector was replaced with a standard photomultiplier tube, allowing accumulation of data with a time resolution of 0.25 ms. The single-wavelength traces were analyzed using the SX18MV software (Applied Photophysics).

For anaerobic experiments, the water bath that controls the temperature of the stopped-flow unit was made anaerobic by addition of sodium dithionite (ca. 20 mM), buffered with sodium phosphate to keep the pH near neutral. Before the experiment, drive syringes and internal tubing were incubated for several hours at room temperature with 50 mM potassium phosphate buffer (pH 7.3) containing D-glucose (ca. 3 mM) and glucose oxidase and catalase (ca. 0.5 and 0.1 μM, respectively) to remove oxygen. Samples were made anaerobic by several cycles of evacuation followed by flushing with argon passed through an Oxisorb (Messer Griesheim) column.

Protein Purification. CCCC, CCAA, and ACAA were purified as previously described (*1*, *9*). The CCCC enzyme used in this work is identical to the Ala10Ala13 mutant described previously (*7*). All enzyme samples were stored at −20 or −70 °C in 50 mM potassium phosphate buffer (pH 7.3) with a slight excess of free FAD and ca. 5 mM DTT. Immediately before being used, the enzyme samples were separated from DTT and excess FAD by gel filtration through a Sephadex G-25 column (1 × 12 cm) and were stored on ice. In the case of the CCCC enzyme, gel filtration yields pure activated E_{ox}, in which the C-terminal cysteines are reduced. Nonactivated E_{ox}, in which the C-terminal cysteines form a disulfide bridge (Scheme 1), was obtained by storing the activated enzyme in excess of 72 h at 6 °C under sterile conditions. For the multiple-turnover experiments, EH_2·NADPH was prepared by addition of an excess of anaerobic NADPH to an anaerobic solution of enzyme in a tonometer. For the single-turnover experiments, the anaerobic enzyme was first titrated to EH_2 with sodium dithionite, followed by anaerobic addition of 1 equiv of NADPH. EH_4 was generated by titration with dithionite. Except for the cases described in the following section, enzymes were not treated with chymotrypsin.

Clipped Enzymes. CCCC and CCAA samples used in the multiple-turnover reaction with $HgBr_2$ were treated with chymotrypsin as described by Fox and Walsh (*2*). This eliminates the possibility of Hg(II) binding to the N-terminal cysteines, Cys10 and Cys13, in the mutant enzyme.

Extinction Coefficients. The extinction coefficient of the E_{ox} form of CCCC was determined using the TCA method described by Mayhew and Massey (*10*); a value for ϵ_{458} of 10.8 ± 0.2 mM^{-1} cm^{-1} was found. For CCAA, the same value was used. For ACAA, extinction coefficients ϵ_{430} and ϵ_{434} of 8.5 (*3*) and 8.7 mM^{-1} cm^{-1} were used at pH 9.2 and 8.0, respectively.

RESULTS

Reactions with $HgBr_2$

Reaction of CCCC and CCAA MR, under Multiple-Turnover Conditions. Panels A and B of Figure 1 show the decrease at 341 nm (i.e., consumption of NADPH) that is observed upon rapid mixing of EH_2·NADPH (concentrations after mixing of ≈10 μM enzyme and ≈100 μM NADPH) with different concentrations of $HgBr_2$ at 3 °C in a stopped-flow spectrometer. Panels A and B depict traces for the CCCC and CCAA enzymes, respectively. Independent of the enzyme-catalyzed reaction, $HgBr_2$ undergoes reaction with NADPH, probably like $HgCl_2$ (*11*), which also leads to a decrease in absorbance at 340 nm. At 100 μM NADPH and 40−1000 μM $HgBr_2$, this background reaction results in absorbance decreases of ca. 0.0036−0.0076/100 ms at 341 nm. Rates of turnover, k_{obs}, obtained from the slopes of the traces and corrected for the appropriate background rate are plotted versus $HgBr_2$ concentration in Figure 1C. Three points emerge from the data. (1) Within error, the rates observed for the CCCC and CCAA enzyme are the same (Figure 1C). This clearly demonstrates that in the case of $HgBr_2$, the C-terminal cysteine pair (C557C558) is not required for full catalytic activity. (2) The observed maximum rates of ca. 18 s^{-1} for turnover of Hg(II) (apparent k_{cat}) are very rapid and ca. 10-fold faster than those observed under standard assay conditions using the wild type enzyme and $Hg(Cys)_2$ as the substrate ($k_{cat} \sim 1.7$ s^{-1}, not shown). (3) The maximum rates are observed when an excess of ca. 5−8 equiv of $HgBr_2$ over enzyme is used. With further increases in substrate concentration, increasing inhibition is observed (Figure 1C). At 600 μM $HgBr_2$ (≈60 equiv), virtually no turnover is observed. It is noteworthy that inhibition in these reactions is very rapid and occurs within the dead time of the stopped-flow spectrometer, as no change in the rate of NADPH consumption over time is observed. This can clearly be seen from the traces for 300 μM $HgBr_2$ (Figure 1A,B), which exhibit ca. 65% inhibition throughout the time interval shown.

The spectral changes in the visible region occurring during these reactions are depicted in panels A and B of Figure 2. The spectrum of the premixing species EH_2·NADPH (Figure 2A,B, solid lines) is characterized by a flavin main band centered at ≈444 nm and a long-wavelength band at ≈530 nm. The latter band arises from two charge transfer (CT) interactions, one on the si side of the flavin involving the anion of Cys140 as the electron donor and the flavin isoalloxazine ring as the acceptor and the other on the re side between the dihydropyridine ring of NADPH acting as

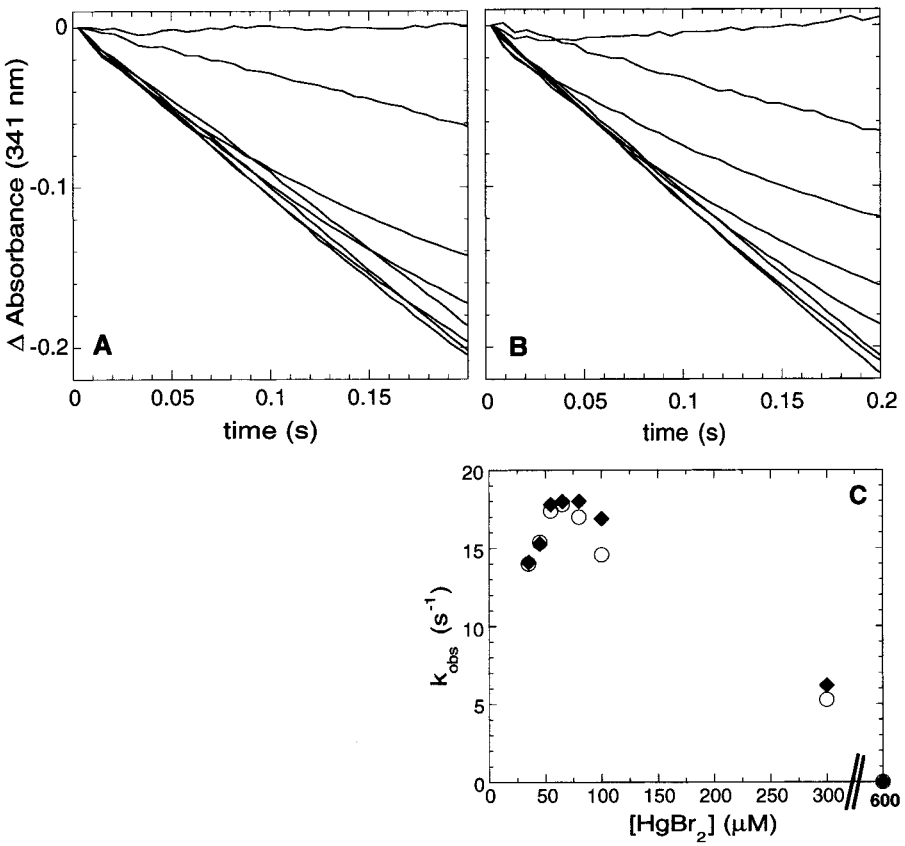

FIGURE 1: (A) Absorbance changes at 341 nm after mixing the EH_2·NADPH complex of CCCC with varying concentrations of $HgBr_2$. Final concentrations were 10.1 μM CCCC and 100 μM NADPH. In decreasing order of *y*-intercept at $t = 0.2$ s, the traces reflect final $HgBr_2$ concentrations of 600, 300, 35, 45, 100, 55, 80, and 65 μM. The experiment was performed at 3 °C in 50 mM potassium phosphate (pH 7.3). (B) Same conditions as in panel A, except using the CCAA enzyme. Final concentrations were 10.3 μM CCAA and 110 μM NADPH. In decreasing order of *y*-intercept at $t = 0.2$ s, the traces reflect final $HgBr_2$ concentrations of 600, 300, 35, 45, 55, 100, 65, and 80 μM. (C) Observed rates calculated from the slopes of the traces in panels A and B, on the basis of an extinction coefficient of 6.22 mM^{-1} cm^{-1} for NADPH and the enzyme concentrations given above: (○) CCCC and (◆) CCAA.

the donor and the flavin isoalloxazine ring acting as the acceptor.[3] Consequently, removal of the reduced pyridine nucleotide leads to a decrease of only ca. 50% in the intensity of the CT band, the remainder stemming from the Cys140−flavin interaction. Likewise, only a partial loss in intensity is observed in the NADPH complex when the negative charge on Cys140 is quenched, e.g., by oxidation (ref *12* and see below), protonation (*13*), or binding of Hg(II) (*14*).

The time-resolved spectral changes occurring upon mixing of EH_2·NADPH with $HgBr_2$ (≈10, ≈100, and 65 μM final concentrations for enzyme, NADPH, and $HgBr_2$, respectively) are essentially the same for CCCC and CCAA (Figure 2A,B). They can be separated into three portions. In the first, very rapid, multiphasic portion that occurs partly during the dead time[4] of the stopped-flow instrument and is essentially complete at $t = 15$ ms, the flavin main band initially becomes more resolved (with a λ_{max} of 452 nm, curve B) and then undergoes a red shift to give a species with a λ_{max} of 458 nm (Figure 2A,B, curve C). At the same time, ca. 60% bleaching of the charge transfer band at 530 nm and a red shift of the remaining charge transfer absorption to a λ_{max} of ≈605 nm are observed. These changes are highly suggestive of the loss of charge on Cys140, and thus, of disruption of the Cys^-−flavin charge transfer interaction due to binding of Hg(II). In fact, the spectrum at $t = 14$ ms (curve C) is, with respect to the shape and position of the absorption bands, nearly identical to those of NADPH complexes of mercuric reductase in which no negative charge on Cys140 is present, such as EH_2·NADPH at low pH (*13*) where Cys140 is protonated and E_{ox}·NADPH where Cys140 forms a disulfide bridge with Cys135 (see below).

Following the first rapid phase, a "quasi steady state phase" ensues over a time interval of at least 150 ms, during which very little change occurs in the visible region. This can be seen by comparison of the spectra taken at $t = 14$ and 130 ms (Figure 2A,B, curves C and D) and is further illustrated

[3] The absorption band at 530 nm in EH_2·NADPH is similar to that in unliganded EH_2, where it is due only to the thiolate−FAD interaction; however, the extinction coefficient is approximately doubled in the complex. The interpretation in the text requires that the NADPH−FAD charge transfer transition occur at a higher energy (shorter wavelength) in the presence of the thiolate−FAD interaction versus that in its absence. This idea is consistent with the observation that the energy of charge transfer transitions is sensitive to the surrounding electronic environment. As an alternative explanation, the enhanced extinction of the band in the complex may be due to changes in the spatial orientation of FAD and/or thiolate upon binding of NADPH. In either case, the intensity of the band is unique to the presence of both NADPH and the unliganded thiolate; hence, the interpretations of the spectral changes are consistent with either explanation.

[4] When data collection was performed using the diode array detector, some indeterminacy regarding the dead time of the measurement occurs. In the case of the fastest access mode, collection of the first spectrum is set by default to an average time value *t* of 1.25 ms in the data collection software. However, the actual recording of the first spectrum deviates by up to ±2.54 ms from this value.

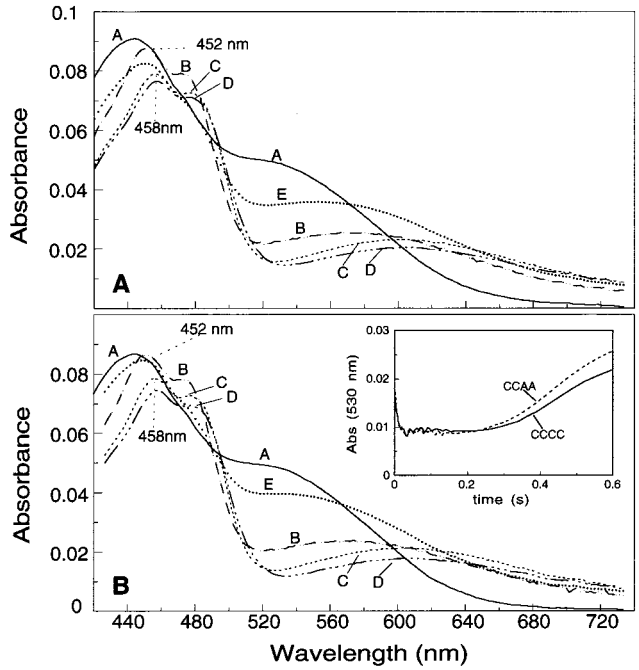

FIGURE 2: Selected spectra in the visible region recorded during the reaction of EH_2·NADPH (same enzyme and NADPH concentrations as in Figure 1) with $HgBr_2$ (65 μM final concentration). (A) For CCCC, curves A−E were taken before mixing, at the stop of the syringes (t = 0 ms) and at t = 14, 130, and 1700 ms, respectively. (B) For CCAA, with exception of curve C which was taken at t = 12 ms, curves A−E were taken at the same time points as those shown in panel A. The inset depicts the time-dependent absorbance changes at 530 nm for the two experiments.

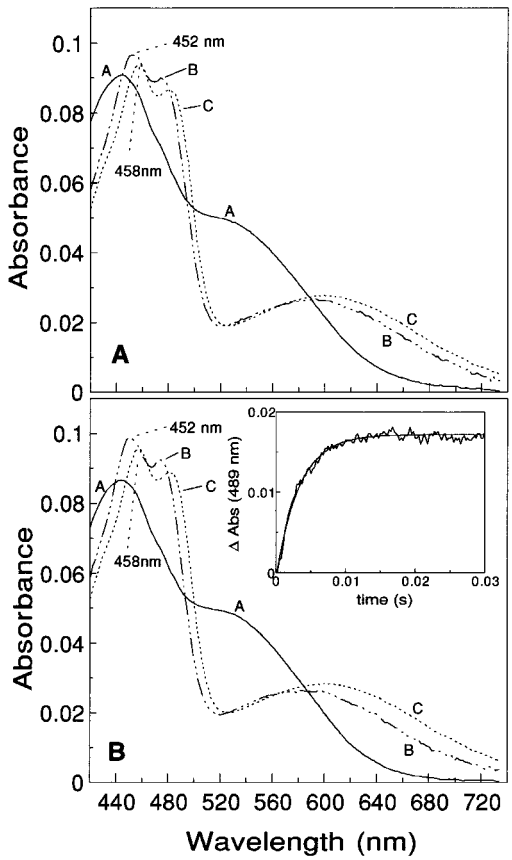

FIGURE 3: Selected spectra in the visible region recorded during the reaction of EH_2·NADPH (same enzyme concentrations as in Figure 1A,B) with $HgBr_2$ (600 μM final concentration). (A) For CCCC, curve A was taken before mixing, B immediately after mixing, and C at $t \approx$ 40 ms. Panel B shows the analogous experiment with CCAA, with spectra taken at the same times as in panel A. The inset shows a typical trace obtained at 489 nm in a single-wavelength experiment with CCAA EH_2·NADPH and $HgBr_2$ at 11.2 and 1000 μM, respectively, after mixing. The smooth line represents a fit to the data with an apparent rate constant of 340 s^{-1}.

by the plateau between t = 20 and ≈200 ms at λ = 530 nm (Figure 2B, inset). From the traces at 341 nm (Figure 1A,B), it is estimated that more than three full turnovers occur during this time period. Thus, the small absorbance changes that do occur may reflect slight changes in the relative levels of NADPH- and $NADP^+$-bound forms as the product accumulates. In the third and final phase, the CT absorbance at 530 nm reappears (Figure 2B, inset) as a consequence of consumption of the limiting substrate $HgBr_2$, yielding a final spectrum with mixed EH_2·NADPH and EH_2·$NADP^+$ character (Figure 2A,B, curves E; *1*).

At 600 μM $HgBr_2$, where no NADPH consumption is observed and both enzymes are fully inhibited, the spectral changes in the visible region over the first 100 ms (Figure 3A,B) are remarkably similar to those under maximum turnover conditions (Figure 2A,B). (After 100 ms, no useful information could be obtained due to baseline shifts caused by $HgBr_2$-induced protein precipitation under these conditions.) In the first observable spectra for both CCCC and CCAA enzymes (Figure 3A,B, curve B), the flavin main bands have essentially the same resolution and position (λ_{max} = 452 nm) as those observed at 65 μM $HgBr_2$ (Figure 2A,B, curve B). However, the CT bleaching at ≈530 nm, which is indicative of a loss of charge on Cys140 due to binding of the metal ion, is essentially complete within the dead time using 600 μM $HgBr_2$, suggesting a Hg(II) concentration dependence in the first phase at lower concentrations of Hg(II). The only kinetically observable phase at the higher Hg(II) concentrations involves the rapid conversion of the dead time spectra to red-shifted spectra (Figure 3A,B, curve C) that are identical to the "quasi steady state" spectra in Figure 2A,B (curves C) with respect to the position of the flavin main band, shoulders, and the charge transfer band. However, there is one important difference. In the inhibited cases, the intensities of both the charge transfer and flavin main absorbance bands are ca. 20% higher than in the rapid turnover cases. This strongly suggests that during rapid turnover in the steady state phase, at least 20% of the enzyme flavin is reduced and that partial flavin reduction either does not occur or occurs to a lesser extent in the inhibited complexes.

For comparison with the $HgBr_2$ data, we also performed multiple-turnover experiments with both the CCCC and CCAA enzymes using $Hg(SCN)_2$ as the substrate. This compound has an overall stability constant comparable to that of $HgBr_2$, but much lower than the constants for $Hg(CN)_2$ or $Hg(SR)_2$ [$HgBr_2$, log K_f = 18; $Hg(SCN)_2$, log K_f = 17.3; $Hg(CN)_2$, log K_f = 35 (*15*); $Hg(SR)_2$, log $K_f \approx$ 39−40 (*16*)]. For the CCCC enzyme, apparent k_{cat} values of 15.1, 12.7, and 2.0 were obtained using 55, 100, and 300 μM $Hg(SCN)_2$, respectively (data not shown). Similarly, CCAA exhibited rates of 14.1, 9.8, and 1.6 s^{-1} for the three respective mercury salt concentrations. Thus, like $HgBr_2$, $Hg(SCN)_2$ is an equally good substrate for both enzymes, and is reduced at a much more rapid rate than $Hg(SR)_2$ under

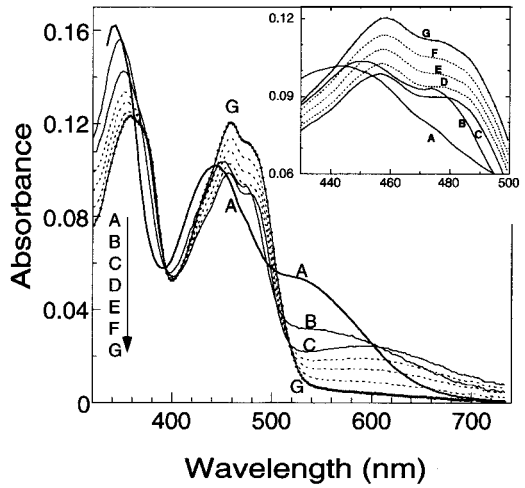

FIGURE 4: Single turnover of CCAA EH_2·NADPH (12.4 μM final concentration for each) with $HgBr_2$ (100 μM final concentration) as monitored in the stopped-flow spectrometer, in 50 mM potassium phosphate buffer at pH 7.3 and 3 °C. Spectrum A is that of EH_2·NADPH. Spectra B−G were taken immediately after the stop of the syringes and at 11.5, 26.9, 42.2, 70.4, and 260 ms, respectively. The inset shows an enlargement of the absorbance changes in the 420−500 nm region.

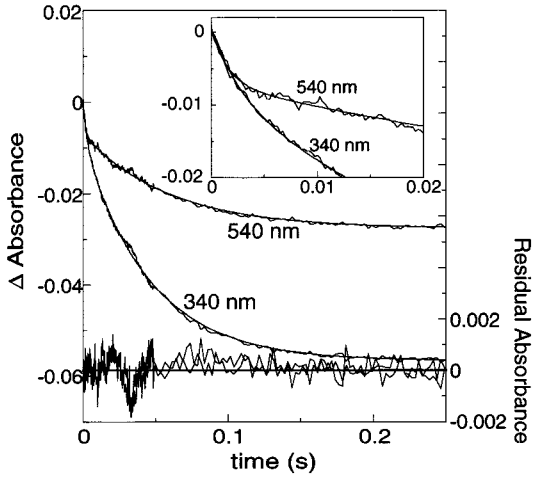

FIGURE 5: Typical absorbance changes at 340 and 540 nm upon rapid mixing of CCAA EH_2·NADPH (11.2 μM final concentration for each) with $HgBr_2$ (100 μM final concentration) using single-wavelength detection and the same buffer and temperature that are described in Figure 4. At both wavelengths, excellent fits (smooth lines) were obtained using two exponentials. The inset shows the rapid changes observed at the beginning of the reaction. At the bottom of the graph, the residual absorbances, obtained from subtraction of the experimental traces from the respective fits at 540 and 340 nm (right-hand *y*-axis), are overlayed. Note that the largest deviations observed between $t = 20$ and 50 ms are due to a pressure release artifact of the stopped-flow instrument. Apparent rate constants determined for the fast process were 590 ± 90 and 590 ± 180 s^{-1} at 540 and 340 nm, respectively. For the slow phase, an average apparent rate of 23.5 ± 1 s^{-1} was determined.

normal turnover conditions. A further parallel to $HgBr_2$ is the observation of inhibition with increasing substrate concentration.

Reaction of CCAA MR, under Single-Turnover Conditions. To obtain a more quantitative picture of the kinetic mechanism, we employed single-turnover conditions using the CCAA enzyme with NADPH as the limiting substrate (stoichiometric with enzyme) and collected spectra at intervals of 2.54 ms, the fastest aquisition mode available for the diode array detector. Figure 4 shows selected spectra taken during the course of the reaction between 100 μM $HgBr_2$ and 12.4 μM EH_2·NADPH. As in the multiple-turnover case (Figure 2A,B), considerable changes occur during the dead time of the experiment, leading to a spectrum (curve B) with the resolved flavin band ($\lambda_{max} \approx 452$ nm) and ca. 40% quenching of the charge transfer absorbance at 540 nm. The remaining rapid changes that occur during the first 12 ms (curve B → C) are complex and, upon close inspection, appear to involve three processes. (1) A further decrease at ≈540 nm indicates that Hg(II) binding to Cys140 reaches completion in this phase. (2) A red shift of ca. 6 nm in the flavin spectrum occurs as observed above. This is clearly a process separate from binding of Hg(II) to Cys140, since it occurs after Hg(II) binding is complete in the inhibited case (shown in Figure 3A,B). (3) A third process is evident from the lower absolute absorbances of the flavin spectra (curves C) in Figures 4 and 2A,B compared to those in Figure 3A,B. The lowered intensity indicates that partial internal reduction (i.e., hydride transfer from complexed NADPH to FAD) is an additional process that takes place in the first few milliseconds of the uninhibited reaction. After the rapid changes, a slow phase ensues (see curve C → G) during which two processes occur. The significant absorbance decrease in the 340 nm region indicates that NADPH consumption, and thus, reduction of complexed Hg(II), occurs in this phase. Concomitantly, the disappearance of the charge transfer band and the increase in the flavin absorbance near 460 nm indicate that following the rate-limiting reduction of Hg(II), elemental mercury rapidly dissociates and excess Hg(II) rapidly rebinds at the active site. The resulting spectrum (curve G) exhibits mixed EH_2·$NADP^+$·Hg(II) and EH_2·Hg(II) character (*14*, *17*), indicating that $NADP^+$ is partially dissociated in the final complex.

To kinetically differentiate the three rapid processes, we could not use the low time resolution of the diode array detector and hence switched to single-wavelength detection using a standard photomultiplier with a time resolution of 0.25 ms (Figure 5). Binding of Hg(II) was monitored at 540 nm, a wavelength that is isosbestic with respect to the red shift, as can be seen in Figure 3. The data are best fit using two exponentials, k_{obs}^{fast} and k_{obs}^{slow}. The fast phase (k_{obs}^{fast}) shows a linear dependence on the $HgBr_2$ concentration (Figure 6A), and the associated amplitudes extrapolated to time zero fully account for the changes occurring during the dead time of the experiment. From these results, we conclude that binding of $HgBr_2$ to Cys140 is limited by a single second-order reaction with a $k_{binding}$ of ≈8×10^6 M^{-1} s^{-1}. The mechanistic implications of this observation will be discussed below. With regard to the non-zero *x*-intercept (at ≈2 equiv of $HgBr_2$) in Figure 6A, we suspect that this is due to rapid nonspecific binding of the highly reactive $HgBr_2$ to surface residues on the protein, resulting in effective $HgBr_2$ concentrations that are lower than the total concentrations plotted in Figure 6A. Further support for this view comes from the observation that a steep decline in the rate of turnover in both CCCC and CCAA is observed at low $HgBr_2$ concentrations (<4 equiv, not shown) and that virtually no rapid turnover can be detected with 1−2 equiv of $HgBr_2$. This behavior strongly suggests that a small amount of Hg(II) binds outside the active site and is not rapidly available

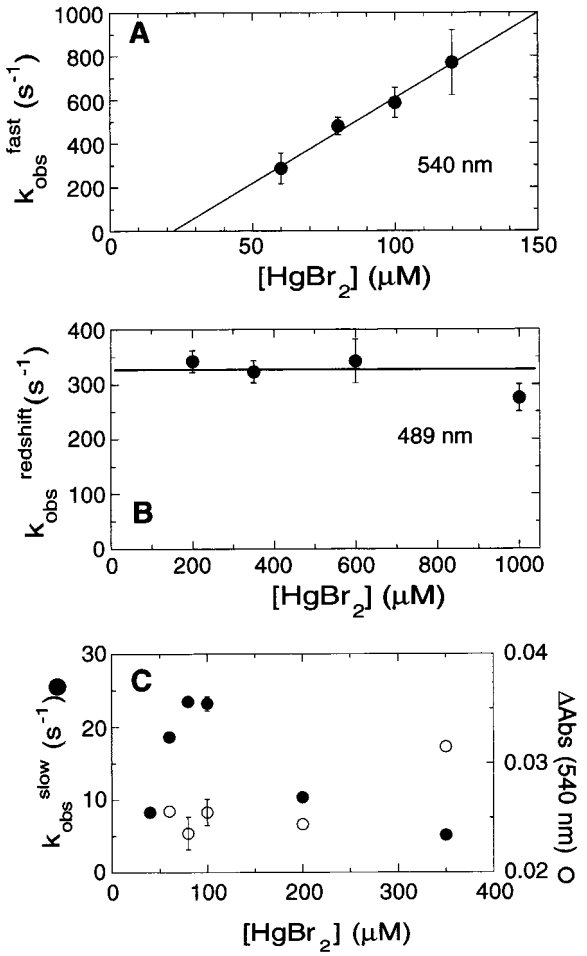

FIGURE 6: Concentration dependence of apparent rate constants obtained from rapid mixing of CCAA EH_2·NADPH with varying concentrations of $HgBr_2$. Panel A shows the variation of the fast phase determined from traces at 540 nm between 60 and 120 μM $HgBr_2$. Panel B depicts the rates obtained from analysis of the monophasic traces at 489 nm (see the Figure 3B inset) between 200 and 1000 μM $HgBr_2$. Panel C shows the rates of the slow phase obtained from diode array data sets subjected to global analysis between 330 and 730 nm (●). Note that the rates obtained from this procedure are consistent with the rates obtained from single-wavelength analysis. The data depicted with ○ reflect absorbance changes at 540 nm associated with the slow phase. Final EH_2·NADPH concentrations were 11.2 μM for panels A and B and 12.4 μM for panel C.

for reduction.

As indicated above, a second fast process involving internal hydride transfer from NADPH to FAD results in decreased absorbance over the entire spectrum and, hence, should also be observable in the traces at 540 nm. Under maximum turnover conditions, it was estimated that up to 20% of the enzyme flavin is reduced. This would yield a maximum absorbance change of ca. 0.006 at 540 nm. However, since no additional rapid exponential had to be invoked to account for the total rapid absorbance change at this wavelength, we can conclude that the rate of internal equilibration to the partially reduced species is at least comparable to binding of $HgBr_2$ at the noninhibitory concentrations.

The third rapid process associated with the red shift of the spectrum is observed at both inhibiting and noninhibiting $HgBr_2$ concentrations. As mentioned earlier, at high $HgBr_2$ concentrations, binding reaches completion within the dead time of the stopped-flow instrument, and internal reduction becomes negligible. Thus, we were able to keep the study of the red shift largely independent of the other processes using $HgBr_2$ concentrations between 200 and 1000 μM. Data obtained from single-wavelength studies at 489 nm (Figure 3B inset) can be fit to a single exponential to yield an average rate constant $k^{redshift}$ of ≈330 s^{-1}, independent of Hg(II) concentration (Figure 6B). The process associated with the red shift clearly occurs after binding of $HgBr_2$ to Cys140, and the simple shift of the spectral features to lower energy transitions indicates that the process results in a slight change in the electronic environment of the active site. As one hypothesis to explain these observations, we propose that the initially observed Hg(II) complex with a λ_{max} of ≈452 nm retains one bromide ligand within the active site at least partially associated with the metal ion. The red shift could then result from dissociation of the ligand from the metal ion and ultimately from the active site. Some support of this interpretation was obtained from analysis of binding of $Hg(CN)_2$ to EH_2·NADPH, which will be described in detail elsewhere. Like that of $HgBr_2$, binding of $Hg(CN)_2$ leads to partial quenching of the charge transfer at 540 nm that is again followed by a red shift of the spectrum. However, the apparent rate constant for the red shift is only ≈50 s^{-1}, some 6−7 times slower than that observed with $HgBr_2$. This ligand dependence of the rate constant for the red shift correlates inversely with the relative affinities of the Hg(II) ligands, which could reflect differences in their relative dissociation rates from an intermediate complex; i.e., the weaker bromide ligand dissociates much faster than the tighter cyanide ligand. It should be mentioned that no firm conclusion regarding the sequence of the three fast processes can be reached from the presented kinetic data alone. While the second-order binding is clearly the initiating event, it is not clear whether the process associated with the red shift precedes internal reduction, or vice versa. However, some clue can be obtained from the position of the charge transfer bands seen in the species involved. In the present case, the charge transfer absorbance is due to an NADPH−FAD interaction in which the pyridine nucleotide functions as the electron donor and the flavin as the acceptor. In studies with Old Yellow Enzyme (*18*) substituted with artificial flavins and phenoxide ligands, it was found that a red-shifted charge transfer band is reflective of a more positive redox potential of the flavin. By analogy, in the present case, the red shift in the charge transfer band of ca. 15−20 nm may reflect a change to a more positive flavin redox potential. Alternatively, the red shift could reflect a more negative NADPH redox potential. Either shift in redox potential is equivalent to a relative stabilization of an internally reduced EH_4·$NADP^+$·Hg(II) enzyme species. On the basis of these considerations, it is likely that significant internal reduction occurs on the level of the red-shifted species rather than on the level of the preceding oxidized enzyme species. We therefore favor a mechanism in which internal reduction occurs after bromide dissociation at noninhibiting concentrations of $HgBr_2$.

In contrast to the fast reactions, which were too fast to be analyzed reliably using diode array data, the slow changes, which were assigned to reduction of Hg(II) and rebinding of excess metal ion (curves C → G in Figure 4 and the main graph in Figure 5), were readily fit to a single exponential

using global analysis over the entire wavelength range. Values of k_{obs}^{slow} obtained using this procedure are plotted in Figure 6C together with the amplitudes of the absorbance changes at 540 nm for each $HgBr_2$ concentration. At 80−100 μM $HgBr_2$, the maximum rate constant for this phase was determined to be ≈23.5 s^{-1}, some 30% higher than the maximum apparent k_{cat} measured in the multiple-turnover experiments (Figure 1C). The discrepancy in these values suggests that another reaction, which could not be observed in the single-turnover experiment, is partially rate-limiting in k_{cat}. This point will be addressed further below. The observation of only one phase for the two processes indicates that the rate of binding of the next Hg(II) is greater than the rate of reduction. Thus, $k_{obs}^{slow} \approx k_{reduction} \approx 23.5\ s^{-1}$. At higher $HgBr_2$ concentrations, inhibition is observed once again. Thus, at 350 μM $HgBr_2$, k_{obs}^{slow} is ca. 20−25% of the maximum rate. However, it should be emphasized that in the inhibited cases where some rate of turnover is still measurable, the absorbance changes at 540 nm that are reflective of the disappearance of the NADPH−FAD CT complex do not decrease as would be expected if a fraction of the enzyme becomes inactivated toward electron transfer (Figure 6C). On the contrary, an increased amplitude is observed, indicative of both the decreased extent of internal reduction that occurs with increased Hg(II) concentrations and ultimately complete consumption of the NADPH at the lower rate. These data strongly suggest that inhibition is not due to fractional inactivation of the enzyme but that the electron transfer itself is slowed within the inhibited complex.

As a final check on the consistency of the data, we also analyzed single-wavelength traces at 340 nm (Figure 5). The overall spectral changes fit nicely to two exponentials. The fast phase accounts for ca. 20% of the total absorbance change, consistent with the assignment of this phase to Hg(II) binding and internal reduction, and exhibits a concentration dependence of the rate constant similar to that found at 540 nm (Figure 6A). The rates for the remaining 80% of the total change are essentially the same as k_{obs}^{slow} obtained from the global fit over all wavelengths (Figure 6C). This observation lends additional support to the interpretation that Hg(II) reduction occurs during the slow phase and is the major rate-limiting step of the reaction.

Reaction of ACAA MR. To further define the mechanistic pathway of $HgBr_2$ reduction during both single and multiple turnover, several points need to be addressed and require additional data. The first of these involves the pathway for binding of $HgBr_2$ to Cys140. The data in Figure 6A indicate that the rate of binding of $HgBr_2$ to Cys140 is limited by a second-order process. This can be interpreted in two ways. Either Cys140 attacks $HgBr_2$ directly, or Cys135 makes the initial, rate-limiting attack followed by very rapid attack of Cys140 on an intermediate enzyme−HgBr complex (Scheme 3). Examination of structural data for the enzyme suggests that Cys135 would be the initially accessible thiol, hence, favoring the second interpretation. To address this issue and determine if Cys135 is required at all for efficient reduction of Hg(II), we examined the reaction of $HgBr_2$ with the ACAA mutant of MR, which retains only Cys140.

In the ACAA mutant, the pK_a of Cys140 is elevated to 6.7, versus ca. 5 in CCCC and CCAA (*3*); hence, the reaction was initially examined at pH 9.2 where Cys140 is fully deprotonated. However, at this pH, increased rates of both

Scheme 3: Alternative Reactions for Binding $HgBr_2$ to Cys135 and Cys140

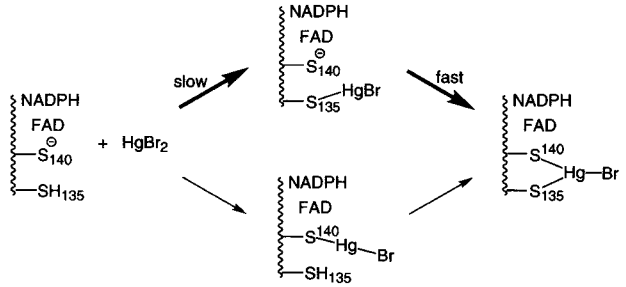

the background reaction between NADPH and $HgBr_2$ and protein precipitation due to nonspecific Hg(II) binding substantially obscure any reactions with the enzyme. To reduce the interference, we examined the reaction at pH 8 where Cys140 is still ca. 95% ionized and the background reactions are slower. At this pH, binding of $HgBr_2$ to Cys140, monitored by disappearance of the CT band, was much slower than with the CCCC or CCAA enzymes. Thus, for the ACAA enzyme, k_{obs} values of 6.3, 30, and 62 s^{-1} were found with 150, 400, and 1000 μM $HgBr_2$, respectively (data not shown), compared with a value of ≈600 s^{-1} for the CCAA enzyme with 100 μM $HgBr_2$ (Figure 6A). In addition to the slower observed rate of binding, no detectable turnover at 340 nm (with a minimal detectable limit above the background reaction of 0.5 s^{-1}) was observed using concentrations between 150 and 6000 μM $HgBr_2$. Thus, turnover in ACAA is at least 35 times slower than in CCCC and CCAA. These data clearly show that Cys135 is required for both rapid turnover and rapid binding of Hg(II) to Cys140 and strongly suggest that in the CCAA enzyme, the initial point of binding of $HgBr_2$ is Cys135 (Scheme 3, top path).

Reaction of Glutathione Reductase. The data for the CCAA enzyme clearly show that only Cys135 and Cys140 are required for catalytic reduction of $HgBr_2$. Since all the other members of the disulfide oxidoreductase family are homologous with respect to this cysteine pair, we also tested the EH_2•NADPH complex of another family member, yeast glutathione reductase, for its ability to reduce $HgBr_2$ (data not shown). Although the spectral changes in the visible region are very similar to those observed for CCCC and CCAA, and indicate rapid binding of the metal ion (160 ± 20 s^{-1} at 30 μM $HgBr_2$), no consumption of NADPH due to reduction of Hg(II) was evident in the spectral changes at 340 nm.

Completing the Catalytic Cycle

To define the remaining mechanistic uncertainties, we now refer to Scheme 4, which incorporates both the conclusions drawn from the above data and several hypothetical pathways for completion of a catalytic cycle. The main pathway from species **I** to species **III** is defined by the results described above. Thus, $HgBr_2$ appears to bind in a two-step process, where k_1 defines the rate-limiting second-order reaction of Cys135 with $HgBr_2$ (≈8 × 10^6 M^{-1} s^{-1}), followed by the rapid attack of Cys140 ($k_3 \gg k_1[HgBr_2]$) to yield species **II** with a λ_{max} of 452 nm. Although these binding steps are thought to be reversible, the extent of reversibility is likely to be very small due to the much greater affinity of Hg(II) for thiolates than for bromide. Species **II** then undergoes

Scheme 4: Alternative Pathways for Reduction of Hg(II)[a]

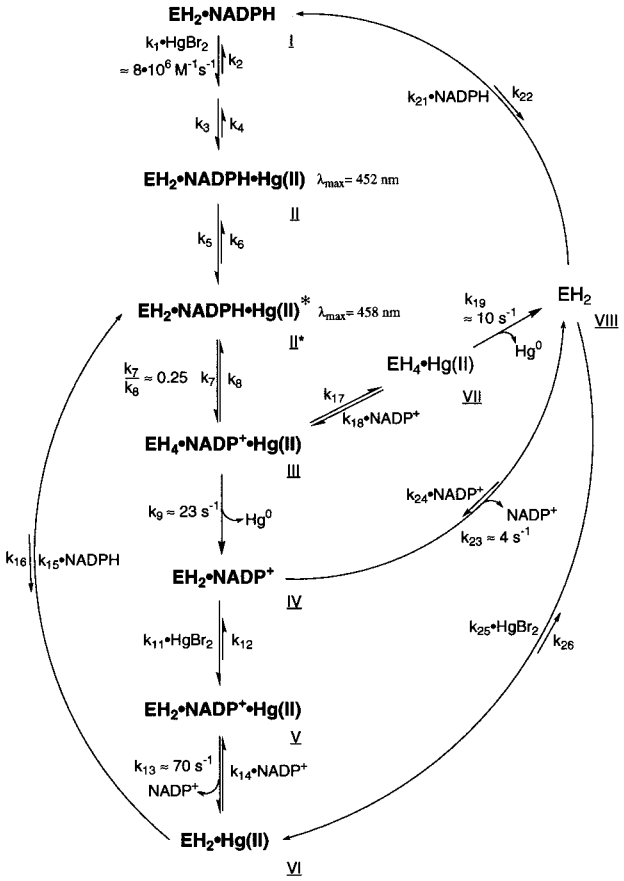

[a] The species along the reaction path identified for the substrate $HgBr_2$ are bold.

the red shift ($k_{obs}^{redshift} \approx k_5 + k_6$), which we have attributed to the loss of the last bromide ligand, and accumulates as a redox equilibrium mixture of species **II*** and reduced species **III** that clearly lies in favor of the oxidized species **II*** (ca. 20% reduced flavin, $k_7/k_8 \approx 0.25$). At noninhibiting concentrations of $HgBr_2$, this redox equilibrium appears to be established very rapidly since we cannot measure an independent rate for this process. However, with inhibiting concentrations of $HgBr_2$, the enzyme appears to accumulate only as species **II***, suggesting that electron transfer at this step has become inhibited. This point will be discussed further below.

Species **III** appears to be the key intermediate from which reduction of bound Hg(II) occurs, but the pathway for reduction and rebinding of substrates during multiple turnover needs to be defined. Several scenarios regarding the remaining sequence of microscopic steps are illustrated in Scheme 4. When the pathway for reduction of Hg(II) is first considered, two scenarios are envisioned. In the first, electron transfer occurs at the level of the EH_4·$NADP^+$·Hg(II) complex (**III**), leading to formation of EH_2·$NADP^+$ (**IV**), which in the single-turnover reaction would simply bind additional $HgBr_2$ and equilibrate between species **V** and **VI**. In the second scenario, $NADP^+$ dissociates first to yield EH_4·Hg(II) (**VII**), followed by reduction of Hg(II) to give unliganded EH_2 (**VIII**), which would then have to rebind both $NADP^+$ and $HgBr_2$ to give the final mixture of **V** and **VI** in the single-turnover experiment.

Reaction of $HgBr_2$ with EH_4. In an effort to distinguish between the two pathways for reduction of bound Hg(II), we examined the reaction of $HgBr_2$ with EH_4 to determine if reoxidation of the flavin in EH_4 occurs with a rate constant that is at least as high as the single-turnover rate of reduction k_{obs}^{slow} ($\approx$19−23 s^{-1}). Over a concentration range of 60−600 μM $HgBr_2$, flavin reoxidation occurred in a single phase with apparent rates ranging from 8 to 11 s^{-1}, indicating no significant second-order dependence. The final spectrum in this monophasic reaction is essentially identical to that of E_{ox}, as expected for the spectrum of EH_2·Hg(II) in the presence of excess Hg(II) (*14*). No accumulation of EH_2 was detected, indicating that binding of excess Hg(II) is very rapid and that the rate of appearance of the oxidized flavin spectrum truly reflects the rate of reduction of the bound metal ion. This rate of 8−11 s^{-1} (k_{19}, Scheme 4) is clearly slower than both the rate of turnover (apparent $k_{cat} \approx 18$ s^{-1}) and the rate of the slow phase ($k_{obs}^{slow} \approx 19-23$ s^{-1}) under single-turnover conditions. In addition, no inhibition was observed at the high $HgBr_2$ concentrations, while complete inhibition was seen in the turnover experiments starting from EH_2·NADPH. These results rule out the second pathway for reduction of Hg(II) and indicate that EH_2·$NADP^+$ (**IV**) must be an intermediate in the catalytic turnover.

Returning to Scheme 4, we envision two alternative pathways for species **IV** to continue in the catalytic cycle. In the first scenario, pyridine nucleotide exchange would occur prior to binding of the next $HgBr_2$. The viability of this pathway requires that dissociation of $NADP^+$ from EH_2·$NADP^+$ (**IV**) and rebinding of NADPH are both faster than the apparent k_{cat}. In the second scenario, binding of the next metal ion to Cys140 in EH_2·$NADP^+$ (**IV**) precedes dissociation of $NADP^+$. In this case, removal of the charge−charge interaction between the Cys140 thiolate anion and the positively charged $NADP^+$ across the flavin could weaken the binding of $NADP^+$, leading to partial dissociation of $NADP^+$ (species **VI**) as was observed in the final spectrum of the single-turnover experiment. Binding of NADPH to **VI** would then lead to **II** or perhaps **II*** if full exchange of the Hg(II) ligands has already occurred at the level of species **V** or **VI**. The viability of this pathway requires that the rates of both binding steps for $HgBr_2$ and NADPH, as well as the dissociation of $NADP^+$ from EH_2·$NADP^+$·Hg(II) (**V**), all be at least as fast as the apparent k_{cat}. The data from the single-turnover experiment (Figure 4) clearly demonstrate that binding of the next $HgBr_2$ is very rapid since no accumulation of EH_2·$NADP^+$ (**IV**) was observed. Furthermore, binding of NADPH to any form of the enzyme lacking a pyridine nucleotide ligand is complete in $\leq$3 ms and, hence, is much more rapid than turnover (ref *12* and unpublished observations). Thus, the key distinction between these pathways is the relative rates of dissociation of $NADP^+$ from EH_2·$NADP^+$ (**IV**) versus that from EH_2·$NADP^+$·Hg(II) (**V**), and whether either is in agreement with the apparent k_{cat}.

Reaction of E_{ox} with NADPH. The feasibility of the first pathway can easily be examined in the reaction of E_{ox} with NADPH. Previous studies at 5 °C (*12*) have shown that rapid mixing of E_{ox} and NADPH leads to formation of E_{ox}·NADPH in $\leq$3 ms, followed by chemical conversion to EH_2·$NADP^+$ (**IV**) and subsequent conversion to EH_2·NADPH (**I**) in the presence of >1 equiv of NADPH. This final reaction,

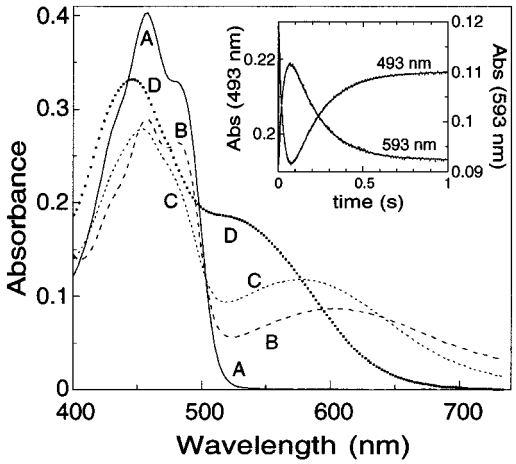

FIGURE 7: Results of rapid mixing of CCCC (nonactivated E_{ox}) and NADPH (37.25 and 150 μM, respectively, after mixing) in the stopped-flow spectrometer, in 50 mM potassium phosphate buffer at pH 7.3 and 3 °C. All spectra, except that of E_{ox} (curve A), are those of the pure species obtained from SVD of the raw data and a fit to two exponentials using the program ProK from Applied Photophysics. Curves B−D are assigned to E_{ox}·NADPH, EH_2·$NADP^+$, and EH_2·NADPH, respectively. The inset shows absorbance changes vs time at 493 and 593 nm; the solid lines through the data points reflect the best fit to two exponentials with k_{app} values of ≈31 and 5.8 s^{-1}.

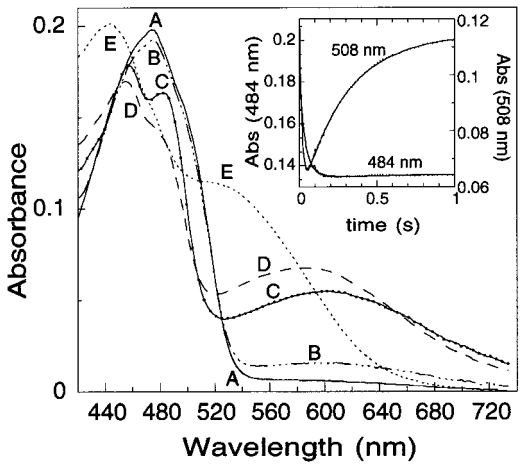

FIGURE 8: Results of rapid mixing of activated E_{ox}·$NADP^+$ (22.3 and 300 μM) with 3 mM NADPH (final concentrations). All spectra, except that of E_{ox}·$NADP^+$ (curve A), are those of the pure species obtained from SVD of the raw data and a fit to three exponentials using the program ProK from Applied Photophysics. Curves B−E correspond to the dead time spectrum and the spectra of E_{ox}·NADPH, EH_2·$NADP^+$, and EH_2·NADPH, respectively. The inset shows the absorbance changes vs time at 508 and 484 nm; the solid lines through the data points reflect the best fit to three exponentials with k_{app} values of 71, 29, and 4.8 s^{-1}.

which is exactly that proposed in the first pathway above, was reported by Sahlman et al. (*12*) to occur with a rate constant of 7.8 s^{-1} (5 °C), independent of NADPH concentration, indicating that this is the rate constant for dissociation of $NADP^+$ from **IV**. We have reexamined the reaction under conditions identical to those of our turnover experiments and found rate constants for conversion of EH_2·$NADP^+$ to EH_2·NADPH (Figure 7, curves C and D, respectively) of 4.1 and 5.8 s^{-1} (k_{23}, Scheme 4) for the activated and nonactivated enzyme, respectiveley. These values are clearly too low to account for the apparent k_{cat} of 18 s^{-1}, indicating that the catalytic cycle with $HgBr_2$ does not involve this pathway.

Pyridine Nucleotide Exchange in E_{ox}·$NADP^+$. At this point, the remaining question is whether the rate of $NADP^+$ dissociation from EH_2·$NADP^+$·Hg(II) (**V**) is sufficiently accelerated to account for the apparent k_{cat} value (18 s^{-1}) that is largely limited by k_{obs}^{slow} (ca. 23 s^{-1}). Unfortunately, direct analysis of the reaction of EH_2·$NADP^+$·Hg(II) with NADPH is not feasible since the complex decays slowly but significantly before mixing with NADPH in the stopped-flow unit [presumably due to a noncatalytically relevant rate of reduction of Hg(II) in this complex (*19*)]. Likewise, the reaction of EH_2·$NADP^+$ with a mixture of NADPH and $HgBr_2$ is also not feasible since $HgBr_2$ reacts directly with NADPH. To develop a model of the reaction, we hypothesized that acceleration of dissociation of $NADP^+$ from an EH_2·$NADP^+$·Hg(II) complex might result upon disruption of the charge−charge interaction between the negative charge on Cys140 and the positively charged $NADP^+$ when Hg(II) binds to Cys140. An analogous situation is found in E_{ox}·$NADP^+$, where the negative charge is also absent because Cys140 forms a disulfide bond with Cys135. We therefore used E_{ox}·$NADP^+$ as a mimic to test whether the rate of $NADP^+$ release is at least as fast as the rate of turnover. As shown in Figure 8, rapid mixing of E_{ox}·$NADP^+$ with NADPH leads to formation of an E_{ox}·NADPH intermediate (curve C) with a rate constant of ≈70 s^{-1} (k_{13}). The process is independent of the NADPH concentration (not shown), indicating that it reflects $NADP^+$ dissociation. Thus, in the absence of the negative charge, dissociation of $NADP^+$ is about 17-fold accelerated compared to dissociation from EH_2·$NADP^+$. Using this estimate of 70 s^{-1} for the rate of dissociation of $NADP^+$ from intermediate **V** in Scheme 4 gives a catalytic mechanism for turnover of $HgBr_2$ (**II*/III → IV → V → VI → II*/III**) with only two kinetically significant steps in k_{cat}; i.e., $k_9 \approx 23$ s^{-1}, and $k_{13} \approx 70$ s^{-1}. Substitution of these values into the resulting expression for k_{cat} [$=k_9k_{13}/(k_9 + k_{13})$] yields a value of 17.6 s^{-1}, consistent with the experimentally determined rate of 18 s^{-1}.

DISCUSSION

The two most important results presented in this paper include the equal catalytic competence of the CCAA mutant and wild type CCCC MR and the ca. 10-fold higher rate for turnover (apparent $k_{cat} \approx 18$ s^{-1}) when $HgBr_2$ is used as the Hg(II) substrate. The first result clearly demonstrates that neither Cys557 nor Cys558 is essential as a ligand in the reducible Hg(II) enzyme complex. In contrast, the spectral changes indicating the loss of negative charge on Cys140 upon binding of Hg(II), as well as the lack of activity of the ACAA mutant, strongly suggest that Cys135 and Cys140 comprise the minimum structural elements required for formation of a reducible Hg(II) complex. In addition, comparison of the rates of Hg(II) binding to CCAA versus ACAA indicates that binding of $HgBr_2$ occurs via the initial rate-limiting attack of Cys135 followed by rapid reaction with Cys140 (Scheme 3). In light of these results, what then is the essential role of Cys557 and Cys558 in the in vivo and standard assay settings?

The key difference between the conditions in the studies presented here and in the in vivo and standard assay settings is the nature of the HgX_2 substrate. Because of the very high affinity of Hg(II) for thiols compared with those of other ligands, and the relatively high concentration of thiol-

containing compounds in bacterial cytoplasm (e.g., glutathione or various protein cysteines), the substrate for MR in vivo must be some type of $Hg(SR)_2$ complex. The standard assay mimics this condition through the inclusion of a thiol-containing compound such as cysteine or 2-mercaptoethanol (typically at 1 mM); the presence of external thiols is actually required to prevent both the reaction of weakly liganded HgX_2 compounds with NADPH and inhibition of MR. How then do $Hg(SR)_2$ and $HgBr_2$ complexes differ?

One factor that may affect their initial site of reaction with the enzyme is the difference in their overall shape and volume. In all two-coordinate complexes of Hg(II), the liganding atoms are linearly disposed. With simple atomic ligands such as bromide, this yields a compact, cylindrical structure. However, the thiol-containing ligands have several atoms beyond the Hg(II)-bound sulfur, resulting in a bulkier structure for $Hg(SR)_2$ complexes. This may limit direct access of $Hg(SR)_2$ complexes to the redox-active cysteines (135 and 140), which crystal structure data show emanate from a helix held rigidly near the flavin, well within the active site cavity (*5*). Preliminary data in fact indicate that binding of $Hg(Cys)_2$ to this cysteine pair is kinetically disfavored by several orders of magnitude compared to binding of $HgBr_2$ and $Hg(CN)_2$. It is therefore conceivable that the C-terminal cysteines (557 and 558) are required to mediate access. These residues are found on a rather flexible arm (high temperature factors in the structural data) that may allow sufficient movement to facilitate exchange of one or both of the bulkier $Hg(SR)_2$ ligands for the C-terminal thiols, followed by internal transfer to Cys135 and Cys140. Using the substrate $Hg(ME)_2$, the lower catalytic efficiency of the CCAC compared to the CCCA mutant (*8*) then suggests that Cys557 is particularly important in mediating this internal transfer. This idea is consistent with the observation from crystal structure data that Cd(II), a competitive inhibitor of MR, is liganded strongly in the active site by residues equivalent to Cys557′ and Cys135, and more weakly by the hydroxyl oxygens of Tyr193 and Tyr534′ (*5*).

In view of a potentially altered pathway for bulkier substrates, the second key result that turnover with $HgBr_2$ (apparent $k_{cat} \approx 18\ s^{-1}$) is ca. 10-fold faster than that with $Hg(Cys)_2$ ($k_{cat} \approx 1.7\ s^{-1}$, not shown) is perhaps not surprising. Provided that both substrates $HgBr_2$ and $Hg(Cys)_2$ ultimately undergo reduction from identical complexes with bidentate coordination of the metal ion to Cys135 and Cys140, the overall lower rate of turnover of $Hg(Cys)_2$ may be due to rate-limiting ligand exchange reactions and internal passage to the reduction site. Alternatively, if interaction with $Hg(Cys)_2$ leads to a reducible complex different from that found with $HgBr_2$, it is possible that the low rate of turnover (partly) reflects a higher energy barrier for reduction of the metal substrate. These hypotheses will be addressed in more detail in a forthcoming paper.

As described in the results, the spectral properties of the red-shifted species in Figure 4 indicate that the charge on Cys140 has been quenched in this intermediate. One piece of evidence supporting this interpretation is that the spectrum is quite similar to that of E_{ox}·NADPH where Cys140 lacks negative charge because it is participating in a disulfide bond

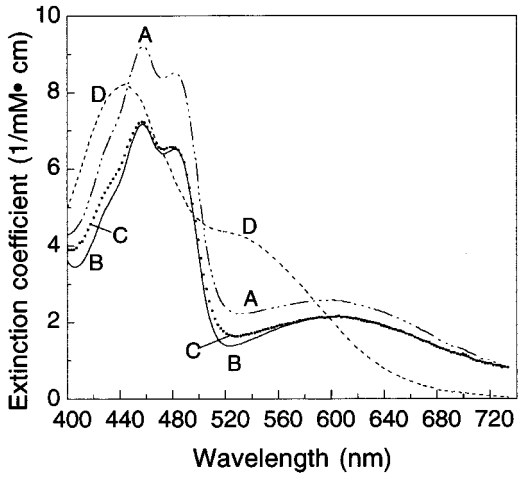

FIGURE 9: Comparison of red-shifted spectral species with E_{ox}·NADPH. Curve A is a spectrum for the red-shifted species (curve C of Figure 3B), obtained at inhibiting $HgBr_2$ concentrations. Curve B is the spectrum of E_{ox}·NADPH (curve B from Figure 7). Curve C is the spectrum of the red-shifted intermediate found at the end of the fast phase in the single-turnover experiment depicted in Figure 4; it was obtained from global analysis of the diode array data set. All spectra were normalized by comparison to their respective EH_2·NADPH spectra. Curve D represents a spectrum of EH_2·NADPH.

with Cys135. A comparison of these spectra, along with the spectrum of the red-shifted intermediate in the inhibited multiple-turnover experiment, is shown in Figure 9. With the striking similarity of these spectra, one might speculate that the red-shifted intermediate is actually E_{ox}·NADPH instead of complex **II*** shown in Scheme 4. However, this would mean that Hg(II) has already been reduced, concomitant with oxidation of Cys135 and Cys140 to a disulfide, in the preceding intermediate since it also appears to lack a charge on Cys140. It would further mean that the following rate-limiting step is just the reduction of the disulfide. Perhaps the strongest argument against this scenario is the overwhelming precedent for complexation of Hg(II) by thiols coupled with the lack of a chemical precedent for reduction of Hg(II) by thiols, particularly at the rate at which it would have to occur to accommodate the second-order dependence of the initial binding step on Hg(II).

The overlay of the spectra in Figure 9 very nicely demonstrates the lower intensity (ca. 20%) of the red-shifted species in the highly active enzyme compared with the red-shifted species in the fully inhibited reaction. This observation indicates that enzyme capable of rapid reduction of Hg(II) accumulates in a redox equilibrium mixture of species **II*** and **III**. Thus, at high concentrations of $HgBr_2$, the higher intensity of the red-shifted species (**II***) suggests that the enzyme can no longer transfer electrons from the bound NADPH to FAD, even though the spectral properties suggest that both the reducible Hg(II) and NADPH appear to be bound similarly. The precise origin of this inhibitory behavior is not known. However, the fact that the protein precipitates at the higher concentrations of $HgBr_2$ used in the inhibitory reactions suggests that an uncertain number of Hg(II) ions can bind nonspecifically to other sites on the protein. In view of the relatively low stability of $HgBr_2$ ($\log K_f = 18$), complexation of Hg(II) by nucleophilic side chains other than thiols is expected. In contrast, when much higher-

affinity compounds, i.e., $Hg(CN)_2$ and $Hg(SR)_2$, are used in millimolar quantities, no such precipitation is observed. The extra binding in the case of $HgBr_2$ could alter both the flexibility of the protein and its electrostatic properties, the latter of which may be particularly important in altering redox equilibria of ligands on the protein. Further examination of this issue is being pursued.

Finally, the mechanism in Scheme 4 appears to explain the results of this work quite well. However, there is one important caveat regarding the mechanistic interpretations of the spectral data leading to this proposal. The underlying assumption leading to Scheme 4 is that the flavins in all of the active sites of MR exhibit identical spectra and reactivities. However, a large body of evidence has previously been presented showing that the active sites on the homodimeric enzyme can in many situations sense the environment of each other and behave asymmetrically with respect to both reactivity and resultant spectral properties (*20*). Although a clear role for the asymmetry in catalysis has not been established, differences in the reduction potentials of the two flavins on the dimers by as much as 35−49 mV have been reported (*6*, *20*). In view of these results, the partial internal reduction described in this work can be interpreted alternatively on the basis of an asymmetric model where two redox potentials are present in the species that precedes Hg(II) reduction, and as a consequence, only one subunit at a time undergoes internal reduction. As the observed absorption signal is always a weighted average of all absorbing species present at both subunits, a rigorous assignment of the individual spectral contributions to each of the subunits is not possible. Therefore, the experimental approach of this work does not allow us to test whether an asymmetry model would be a more apt description of this enzyme system.

ACKNOWLEDGMENT

We thank Emil Pai for sharing the coordinates of MR from *Bacillus* sp. RC607.

REFERENCES

1. Miller, S. M., Moore, M. J., Massey, V., Williams, C. H., Jr., Distefano, M. D., Ballou, D. P., and Walsh, C. T. (1989) *Biochemistry 28*, 1194−1205.
2. Fox, B., and Walsh, C. T. (1982) *J. Biol. Chem. 257*, 2498−2503.
3. Miller, S. M., Massey, V., Ballou, D. P., Williams, C. H., Jr., Distefano, M. D., Moore, M. J., and Walsh, C. T. (1990) *Biochemistry 29*, 2831−2841.
4. Miller, S. M., Ballou, D. P., Massey, V., Williams, C. H., Jr., and Walsh, C. T. (1986) *J. Biol. Chem. 261*, 8081−8084.
5. Schiering, N., Kabsch, W., Moore, M. J., Distefano, M. D., Walsh, C. T., and Pai, E. F. (1991) *Nature 352*, 168−172.
6. Distefano, M. D., Au, K. G., and Walsh, C. T. (1989) *Biochemistry 28*, 1168−1183.
7. Moore, M. J., and Walsh, C. T. (1989) *Biochemistry 28*, 1183−1194.
8. Moore, M. J., Miller, S. M., and Walsh, C. T. (1992) *Biochemistry 31*, 1677−1685.
9. Schultz, P. G., Au, K. G., and Walsh, C. T. (1985) *Biochemistry 24*, 6840−6848.
10. Mayhew, S. G., and Massey, V. (1969) *J. Biol. Chem. 244*, 794−802.
11. Marshall, J. L., Booth, J. E., and Williams, J. W. (1984) *J. Biol. Chem. 259*, 3033−3036.
12. Sahlman, L., Lambeir, A.-M., Lindskog, S., and Dunford, H. B. (1984) *J. Biol. Chem. 259*, 12403−12408.
13. Sahlman, L., Lambeir, A.-M., and Lindskog, S. (1986) *Eur. J. Biochem. 156*, 479−488.
14. Miller, S. M., Massey, V., Ballou, D. P., Williams, C. H., Jr., and Walsh, C. T. (1987) in *Flavins and Flavoproteins*, pp 29−32, Walter de Gruyter and Co., Berlin and New York.
15. Meites, L. (1963) in *Handbook of Analytical Chemistry*, pp 1−39, McGraw-Hill, New York.
16. Stricks, W., and Kolthoff, I. M. (1953) *J. Am. Chem. Soc. 75*, 5673−5681.
17. Moore, M., Distefano, M., and Walsh, C. (1987) in *Flavins and Flavoproteins*, pp 37−40, Walter de Gruyter and Co., Berlin and New York.
18. Stewart, R. C., and Massey, V. (1985) *J. Biol. Chem. 260*, 13639−13647.
19. Sandström, A., and Lindskog, S. (1988) *Eur. J. Biochem. 173*, 411−415.
20. Miller, S. M., Massey, V., Williams, C. H., Jr., Ballou, D. P., and Walsh, C. T. (1991) *Biochemistry 30*, 2600−2612.

BI9808161